Dalton Transactions

ROYAL SOCIETY OF CHEMISTRY

PAPER

View Article Online
View Journal | View Issue

Cite this: *Dalton Trans.*, 2021, **50**, 6857

Graphitic nitrogen in carbon catalysts is important for the reduction of nitrite as revealed by naturally abundant ^{15}N NMR spectroscopy†

Zheng Chen,[a,b] Aleksander Jaworski,[b] Jianhong Chen,[b] Tetyana M. Budnyak,[b] Ireneusz Szewczyk,[c] Anna Rokicińska,[c] Richard Dronskowski,[a,d] Niklas Hedin,[b] Piotr Kuśtrowski *[c] and Adam Slabon *[b]

Metal-free nitrogen-doped carbon is considered as a green functional material, but the structural determination of the atomic positions of nitrogen remains challenging. We recently demonstrated that directly-excited solid state ^{15}N NMR (ssNMR) spectroscopy is a powerful tool for the determination of such positions in N-doped carbon at natural ^{15}N isotope abundance. Here we report a green chemistry approach for the synthesis of N-doped carbon using cellulose as a precursor, and a study of the catalytic properties and atomic structures of the related catalyst. N-doped carbon (NH_3) was obtained by the oxidation of cellulose with HNO_3 followed by ammonolysis at 800 °C. It had a N content of 6.5 wt% and a surface area of 557 m^2 g^{-1}, and ^{15}N ssNMR spectroscopy provided evidence for graphitic nitrogen besides regular pyrrolic and pyridinic nitrogen. This structural determination allowed probing the role of graphitic nitrogen in electrocatalytic reactions, such as the hydrogen evolution reaction (HER), oxygen evolution reaction (OER), and nitrite reduction reaction. The N-doped carbon catalyst (NH_3) showed higher electrocatalytic activities in the OER and HER under alkaline conditions and higher activity for nitrite reduction, as compared with a catalyst prepared by the carbonization of HNO_3-treated cellulose in N_2. The electrocatalytic selectivity for nitrite reduction of the N-doped carbon catalyst (NH_3) was directly related to the graphitic nitrogen functions. Complementary structural analyses by means of ^{13}C and ^{1}H ssNMR, scanning electron microscopy (SEM), transmission electron microscopy (TEM), X-ray diffraction (XRD), X-ray photoelectron spectroscopy (XPS), Raman spectroscopy, and low-temperature N_2 adsorption were performed and provided support to the findings. The results show that directly-excited ^{15}N ssNMR spectroscopy at natural ^{15}N abundance is generally capable of providing information on N-doped carbon materials if relaxation properties are favorable. It is expected that this approach can be applied to a wide range of solids with an intermediate concentration of N atoms.

Received 26th February 2021,
Accepted 12th April 2021

DOI: 10.1039/d1dt00658d

rsc.li/dalton

Introduction

When fabricating carbon materials with tailored functionalities, the structure–property relationship at the atomic level should be considered.[1–8] These considerations are important for the synthesis of metal-free and carbon-based catalysts, where the activity stems from the enhanced exposure of the structural features being catalytically most active.[9–17] The absence of metal-containing entities has intensified the consideration of metal-free carbon catalysts as "green" catalysts.[18,19] The physical and chemical properties of carbon catalysts can be altered by modifying their surface states with carbon–oxygen bonds,[20,21] which in turn modifies their catalytic activity. Another approach to modify the catalytic activity of carbon is to incorporate dopants into the bulk carbon structure, such as doping with nitrogen.[22–28] Although it has been postulated that any element applied as a dopant would improve the catalytic activity,[29–37] a control of the dopant distribution at the atomic level is key to bridging the gap between the atomically precise understanding of homogeneous catalysts and the materials chemistry of heterogeneous

[a]*Institute of Inorganic Chemistry, RWTH Aachen University, 52056 Aachen, Germany*
[b]*Department of Materials and Environmental Chemistry, Stockholm University, 10691 Stockholm, Sweden. E-mail: adam.slabon@mmk.su.se*
[c]*Faculty of Chemistry, Jagiellonian University, Gronostajowa 2, 30-387 Krakow, Poland. E-mail: piotr.kustrowski@uj.edu.pl*
[d]*Hoffmann Institute of Advanced Materials, Shenzhen Polytechnic, 7098 Liuxian Blvd, Shenzhen, China*

†Electronic supplementary information (ESI) available: Calibration curves; CV curves; selectivity, Faradaic efficiency and NH_4^+ yield; T_1 NMR relaxation curve for ^{13}C; XRD; SEM micrographs; TEM images and XPS N 1s spectra. See DOI: 10.1039/d1dt00658d

catalysts.[38,39] Numerous studies of N-doped carbon atoms for catalysis have been performed; for example, Zhao *et al.* demonstrated that several synthetic approaches for the fabrication of "green" carbon catalysts could be used.[40]

Nitrogen-doped carbon catalysts have indeed emerged as promising heterogeneous catalysts, such as for the hydrogen evolution reaction (HER) and oxygen evolution reaction (OER). Despite the progress in developing N-doped carbon catalysts, the structural determination of nitrogen positions at the atomic level has remained highly challenging. The lack of analytical methods for this structural determination has rendered the interpretation of catalytic activity elusive.[41–43] As nitrogen and carbon are neighbors in the periodic table, they are difficult to distinguish by scanning transmission electron microscopy with energy dispersive X-ray spectroscopy (STEM EDX) mapping,[43,44] and in this spectroscopy there is also a problem with choosing the representative spots of the sample.

The local structures of the nitrogen atoms in N-doped carbons can be studied by ^{15}N ssNMR, and by typically enriching the carbons in ^{15}N.[45–47] The obvious disadvantages of ^{15}N labeling are the higher costs accompanied by more complexity of synthesis, particularly for methods using NH_3. Only a few ^{15}N ssNMR studies using N-doped carbon materials at the natural abundance of ^{15}N have been reported in the literature including the study by Fang *et al.*, and our very recent study.[48,49] In the latter, we reported the synthesis of N-doped mesoporous carbon by using porous silica as a template and sugar as a carbon precursor.[49] Upon treatment with HNO_3 and carbonization under a flow of NH_3, followed by the dissolution of the silica template in hydrofluoric acid (HF), an N-doped carbon catalyst with 3.7 wt% of N was produced. ^{15}N ssNMR spectroscopy at natural ^{15}N isotope abundance revealed that N was present in pyrrolic and pyridinic moieties.

Since HF is toxic, we here explore a comparably sustainable route to the synthesis of N-doped carbons and circumvent the applications of HF, and we also involve a renewable cellulose substrate as the carbon precursor.[50–56] The synthetic pathway is illustrated in Scheme 1. It does not cover all principles of *Green Chemistry*,[57] as NH_3 is toxic, however, NH_3 is a common base chemical and allows the introduction of high amounts of N. We report an unexpected incorporation of graphitic N in the N-doped carbon and its detection by using ^{15}N ssNMR spectroscopy. Among the two studied catalysts, the N-doped carbon derived *via* ammonolysis shows the highest catalytic activities in electrochemical reactions, such as the HER, OER and nitrite reduction, and the role of graphitic N is assessed.

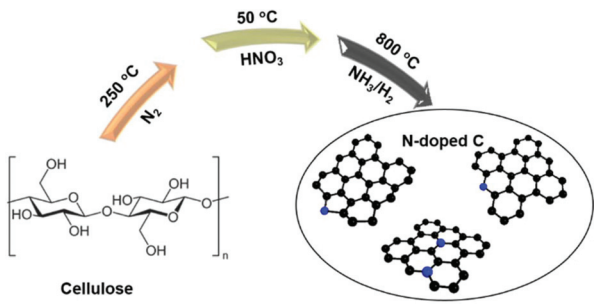

Scheme 1 Schematic illustration of the synthesis to create N-doped carbons. Before the introduction of nitrogen into the structure, the cellulose was dried at 250 °C under an inert atmosphere.

Experimental

Synthesis

Cellulose (microcrystalline, AquaBioSolve Stockholm AB) was used as a carbon source and the main raw material in the synthesis of two types of N-doped carbons. 3.0 g of cellulose was placed into a crucible and then dried in a tube furnace under a N_2 flow (40 mL min^{-1}) at 250 °C for 6 h. The dried product was oxidized by immersing it in a 30 mL of HNO_3 solution (40 wt%) at 50 °C for 3 h. The resultant suspension was centrifuged and washed with deionized water until neutral pH was achieved, before being dried at 120 °C for 8 h under ambient conditions. For carbonization, 1 g of the obtained yellow product was placed into an alumina crucible in a tube furnace and then carbonized under a flow of NH_3 (15 mL min^{-1}) with H_2 (5 mL min^{-1}) at 800 °C for 2 h, at a heating and cooling rate of 10 °C min^{-1}. The NH_3 : H_2 ratio has been chosen based on our experience with metal (oxy)nitride formation.[58,59] The addition of H_2 shifts the equilibrium more toward NH_3 instead of N_2 at such elevated temperatures. The resulting modified carbon was marked as N-doped C (NH_3). Similarly, the complementary carbon obtained under the flow of N_2 (40 mL min^{-1}) was labelled as N-doped C (N_2).

Characterization

N_2 adsorption. N_2 adsorption analyses were conducted at −196 °C using an ASAP 2020 instrument (Micrometrics) for the samples previously degassed at 250 °C for 4 h under dynamic vacuum. The recorded data were analyzed using the following models: Brunauer–Emmett–Teller (surface area, S_{BET}), Langmuir (surface area, $S_{Langmuir}$), *t*-plot (micropore volume, V_{micro}), and Barrett–Joyner–Halenda (mesopore volume, V_{meso}). Moreover, the total pore volume (V_{total}) was determined by the single point method ($p/p_0 \sim 0.99$).

Powder X-ray diffraction (PXRD). PXRD measurements were performed in transmission mode on an STOE STADI-P diffractometer (Cu $K_{\alpha 1}$ radiation) using a DECTRIS Mythen 1 K detector at a scan rate of 1° min^{-1} in a 2θ range from 10° to 60°.

Raman spectroscopy. A LabRAM HR 800 Raman instrument equipped with a spectrograph having an 800 nm focal length was used for the Raman spectroscopic study. The detector was an air cooled (−70 °C) and back thinned CCD detector with 1024 × 256 pixels and a spectral range of 200–1050 nm. The laser used was an air cooled and double frequency Nd:YAG laser (532 nm/50 mW) whose intensity was adjusted by using a filter wheel with 6ND filters which was software controlled.

Electron microscopy (EM). Scanning electron microscopy (SEM) micrographs were recorded using a Leo Supra 35VP SMT (Zeiss) thermal field emission scanning electron micro-

scope. Transmission electron microscopy (TEM) images were recorded using a JEOL 2100F microscope.

Elemental analysis. A Flash 2000 elemental analyzer containing a thermal conductivity detector and an autosampler was used to determine the content of C, N, and H. The quantitative analysis of the metal content in the carbon materials was carried out by inductively-coupled plasma optical emission spectrometry (ICP-OES).

X-ray photoelectron spectroscopy (XPS). The surface composition of the carbonized samples was investigated by XPS using a system constructed by Prevac, equipped with a hemispherical analyzer (VG SCIENTA R3000) and a monochromatized aluminum source Al K_α (E = 1486.6 eV). No charge compensation was needed for the conductive samples. The Au 4f reference peak at 84.0 eV was used for the calibration of the binding energy scale. The collected spectra were analysed using the CasaXPS software.

ssNMR. Magic-angle-spinning (MAS) NMR experiments were performed at a magnetic field of 14.1 T (Larmor frequencies of 600.12, 150.92, and 60.83 MHz for ^{1}H, ^{13}C, and ^{15}N, respectively) using a Bruker Avance-III spectrometer with a wide-bore magnet. The ^{1}H MAS NMR spectrum was acquired using a 1.3 mm probehead and a 60 kHz MAS rate. The acquisition of the ^{1}H MAS NMR spectrum involved the use of a rotor-synchronized, double-adiabatic spin-echo sequence with a 90° excitation pulse of 1.25 μs followed by a pair of 50.0 μs tanh/tan short high-power adiabatic pulses (SHAPs) with a 5 MHz frequency sweep.[49,60,61] Such a pulse sequence was applied to prevent proton background signals and to achieve a flat baseline in the acquired ^{1}H MAS NMR spectrum. All pulses operated at a nutation frequency of 200 kHz, and 64 signal transients were acquired using a relaxation delay of 5 s. Directly-excited ^{13}C and ^{15}N MAS NMR spectra were recorded using a 7 mm probehead and a 7 kHz MAS rate. The ^{13}C acquisition involved a single-pulse (Bloch-decay) protocol with a 90° excitation pulse of 4.0 μs, and 16 384 signal transients were collected using a relaxation delay of 20 s. The ^{13}C NMR chemical shifts were referenced with respect to TMS. The ^{15}N acquisition involved a rotor-synchronized spin-echo sequence with 90° and 180° pulses of 6.5 and 13.0 μs, and 561 800 signal transients were collected with a recycle delay of 1 s (~7 days acquisition time). The ^{15}N NMR chemical shifts are presented with respect to nitromethane. All NMR experiments were performed at natural isotope abundance.

Electrochemical (EC) measurements

For the preparation of an electrode, 5 mg of N-doped C, 30 μL of Nafion (D-520 dispersion 5 wt%, Alfa Aesar), and 970 μL of ethanol were mixed in a glass bottle and dispersed by ultrasound for 30 min. 200 μL of the mixture was subsequently dropped on each side of the carbon fiber substrate (Toray carbon-paper TP-030, Quintech) in a thorough manner, multiple times. The electrode was subsequently obtained after drying the mixture at room temperature for 2 h. The EC experiments were performed with a potentiostat (Gamry instruments) using an electrochemical cell. This electrode, a platinum wire (or carbon paper), and a 1 M Ag/AgCl electrode were used as a working electrode, a counter electrode, and a reference electrode in a three-electrode system, respectively. All current values of the electrodes were recorded at $E_{1M\ Ag/AgCl}$ (V), which can be converted to E_{RHE} (V) using the formula: E_{RHE} (V) = 0.235 (V) + $E_{1M\ Ag/AgCl}$ (V) + [0.059 × pH] (V) at 25 °C. Milli-Q water (18.3 Ω cm) was used to prepare the electrolytes. Linear sweep voltammetry (LSV) and cyclic voltammetry (CV) were performed at a scan rate of 10 mV s^{-1}, and chronoamperometry (CA) was performed at −0.84 V *vs.* RHE for the nitrite reduction reaction. NH_3 was analyzed using the Nessler method and Merck Spectroquant 114423.[62] The amount of nitrite was determined with the 114 658 test kits (MColortest™). The analysis was performed using a UV-Vis spectrophotometer (20 Genesys™) (Fig. S1†). The NO_2^- conversion, selectivity, Faradaic efficiency and NH_4^+ yield of the product were calculated using the following equations:

$$NO_2^-\text{conversion} = \Delta C_{NO2^-}/C_0 \times 100\%$$

$$\text{Selectivity} = (C_{NH4^+}/18)/(\Delta C_{NO2^-}/46) \times 100\%$$

$$\text{Faradaic efficiency} = (6F \times C_{NH4^+} \times V)/(18 \times Q) \times 100\%$$

$$NH_4^+\ \text{yield} = (C_{NH4^+} \times V)/(18 \times t \times m)$$

where ΔC_{NO2^-} is the concentration difference of NO_2^- before and after electrolysis (ppm), C_0 is the initial concentration of NO_2^- (50 ppm), C_{NH4^+} is the final concentration of NH_4^+ (ppm), V is the electrolyte volume (50 mL), F is the Faradaic constant (96 485 C mol^{-1}), Q is the total charge used for the electrode (C), t is the electrolysis time (2 h), and m is the mass of the catalyst (1 mg).

Results and discussion

Catalysis

Doping a carbon-based catalyst with N atoms has been previously shown to enhance the catalytic activity for the OER and HER (*vide supra*),[41,63] although the exact effect of N is still unclear due to the lack of structural information regarding the chemical form of N. It has been suggested that pyridinic N, pyrrolic N and graphitic N with the carbon atoms located at the armchair edge are the intrinsic active sites for the HER and OER.[41,63–65] Here, we investigated two "green" carbon catalysts for the OER, HER and electrochemical nitrite reduction. LSV tests were conducted after extended CV measurements to obtain a stable CV curve (Fig. S2†). The LSV curves are summarized in Fig. 1, which also includes the response of the reference sample of the carbon cloth used as the substrate. N-doped C (NH_3) had the highest amount of N (6.5 wt% based on elemental analysis) and showed higher catalytic activity than N-doped C (N_2).

For the OER, the catalytic activity of N-doped C (NH_3) and N-doped C (N_2) was investigated in 0.05 M H_2SO_4 (pH 1) and 0.1 M NaOH (pH 13) electrolytes (Fig. 1a). The anodic current density generated on the N-doped C (NH_3) catalyst was signifi-

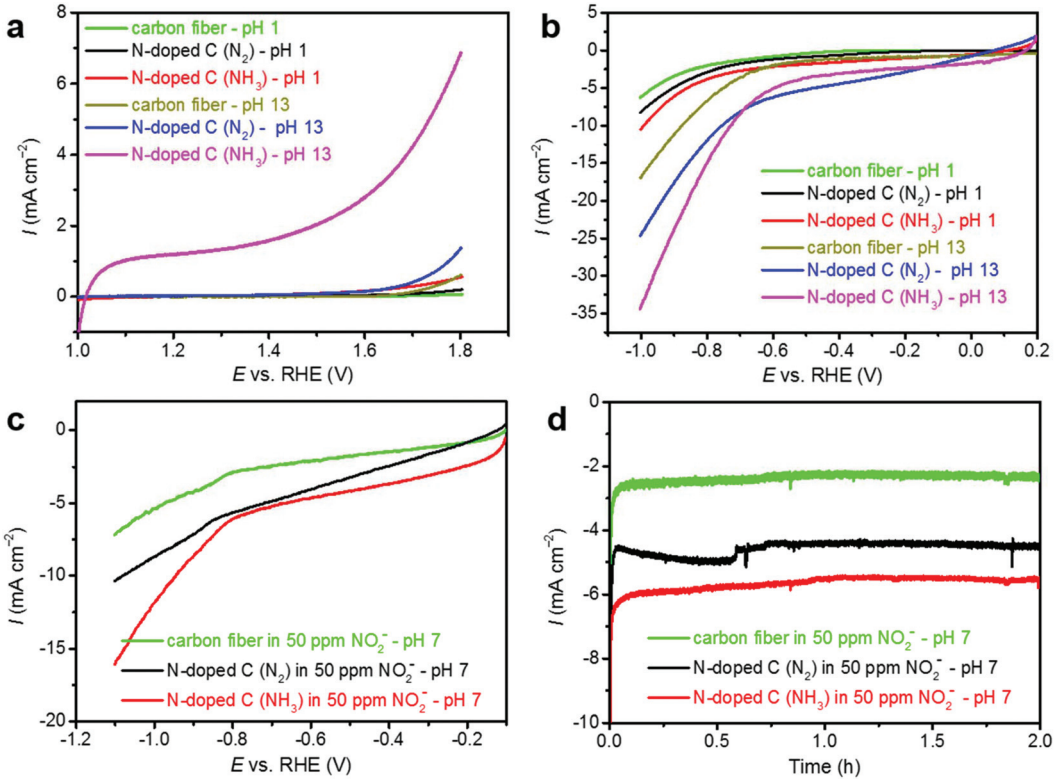

Fig. 1 LSV curves of carbon fiber, N-doped C (N_2) and N-doped C (NH_3) for the OER (a) and HER (b) in a 0.05 M H_2SO_4 (pH 1) electrolyte and 0.1 M NaOH (pH 13) electrolyte; LSV curves (c) and CA at −0.84 V *vs.* RHE (d) of carbon fiber, N-doped C (N_2) and N-doped C (NH_3) for the nitrite reduction reaction in an aqueous electrolyte (0.1 M Na_2SO_4) with 50 ppm of NO_2^-.

cantly higher than those on both N-doped C (N_2) and support (carbon fiber) at high potentials in the NaOH and H_2SO_4 electrolytes. The highest electrocatalytic activity was achieved for the N-doped C (NH_3) sample at pH 13. Under these conditions, the achieved current density of this sample was higher than the sum of all other LSV curves. It should be noted that the current density increase below 1.23 V *vs.* RHE is related to pseudocapacitance. Since N-doped C (NH_3) and N-doped C (N_2) had similar textual properties, the significant enhancement in the activity of the N-doped C (NH_3) catalyst in the OER was related to its much higher N-content, 6.5 wt% *versus* 0.6 wt%. The concentration of the transition metals was <10 ppm.

To further investigate the catalytic activity, we also assessed the HER in 0.05 M H_2SO_4 and 0.1 M NaOH electrolytes (Fig. 1b). A similar trend of superior electrocatalytic activity was observed during the HER for N-doped C (NH_3) as compared with N-doped C (N_2) and the support. However, the differences were not as large as that for the OER. The highest activity was observed under alkaline conditions (pH 13), which indicated that the pyridinic N, pyrrolic N, oxidized nitrogen, NH_2 and graphitic N were activated in N-doped C (NH_3) as in the OER.

To better understand the influence of the N-containing moieties on the selectivity during the electrocatalytic reactions, the electrochemical reduction of nitrite was studied. Our previous report on another type of N-doped carbon catalyst, containing only pyridinic N and pyrrolic N, showed no specific influence on the NH_3 selectivity during the electrochemical reduction of nitrate.[49] The reduction of nitrites is found to follow a similar reduction mechanism to that for nitrates, *i.e.* energetically-favored reduction from nitrate over N_2 and/or NO_x directly to NH_3. We performed electrochemical denitrification in aqueous solutions with 50 ppm of nitrite and 0.1 M of Na_2SO_4. We did not choose higher concentrations, because it is unlikely that wastewater would contain higher concentrations of nitrite. The corresponding LSV curves, and CA experiments performed at −0.84 V *vs.* RHE, are presented in Fig. 1c and d. It should be kept in mind that the amount of generated NH_3 has an influence on the potential *vs.* RHE, but a constant potential value is more realistic for potential commercial applications of nitrite reduction. After CA for 2 h, the N-doped C (NH_3) catalyst showed the highest nitrite reduction efficiency of 58.4%, outperforming the N-doped C (N_2) catalyst and carbon fiber substrate (Table 1).

The selectivity toward NH_3 was the highest for N-doped C (NH_3) (65.6%) when compared to the N-doped C (N_2) catalyst (24.4%) with a lower N content (Fig. S3†). The N-doped C (NH_3) catalyst produced 7.5 ppm of NH_3 from a nitrite concentration of 50 ppm, with the highest Faradaic efficiency of 58.3% and an NH_4^+ yield of 2.63 μmol h^{-1} $mg_{cat.}^{-1}$ (Fig. S3†), while the N-doped C (N_2) catalyst produced only 1.9 ppm of

Table 1 Electrochemical reduction of NO_2^- on carbon fiber, N-doped C (N_2) and N-doped C (NH_3) electrodes in 50 mL of 0.1 M Na_2SO_4 with a 50 ppm NO_2^- electrolyte

Electrode	CA conditions	Initial concentration of NO_2^- (ppm)	Final concentration of NO_2^- (ppm)	Reduction efficiency of NO_2^-	Final concentration of NH_4^+ (ppm)
Carbon fiber	−0.84 V *vs.* RHE for 2 h (pH 7)	50	38.3	23.6%	1.0
N-Doped C (N_2)	−0.84 V *vs.* RHE for 2 h (pH 7)	50	30.1	39.8%	1.9
N-Doped C (NH_3)	−0.84 V *vs.* RHE for 2 h (pH 7)	50	20.8	58.4%	7.5

NH_3. Considering that pyridinic N and pyrrolic N have been shown to not influence the selectivity of the overall nitrite/nitrate reduction, this result indicates that the presence of graphitic N can on the other hand increase the nitrite-to-NH_3 selectivity.

Spectroscopy

To assess the local atomic structure and rationalize the enhanced electrocatalytic activities of N-doped C (NH_3) in the OER, HER, and reduction of nitrite, ssNMR experiments were performed according to our previously described methodology.[49]

For determining the nitrogen positions in the carbon matrix, ssNMR experiments were performed. The ^{1}H MAS NMR spectrum (60 kHz MAS) of the N-doped C (NH_3) sample shows three distinct signals (Fig. 2a). The broad resonance centered at 6.5 ppm originates from the protons terminating the carbon edges. The signal at 1.0 ppm with a shoulder at 1.8 ppm is attributed to the protons present in the –NH_2 and hydroxyl groups. The resonance that shows a rather unusual, negative chemical shift of −2.8 ppm can be assigned to the nucleus-independent chemical shift (NICS) effect on the protons of H_2O molecules confined to the internal cavities of the N-doped C particles.[66–68] This is associated with ring currents that are induced perpendicularly to the plane of the aromatic system of delocalized π electrons in the external magnetic field. Such ring current effects may be responsible for abnormal proton chemical shifts in aromatic systems.[69] The directly-excited ^{13}C MAS NMR spectrum of N-doped C (NH_3) is depicted in Fig. 2b. The single resonance from the sp^2 hybridized carbon atoms shows an isotropic chemical shift of 122 ppm and spinning sideband manifold due to the chemical shift anisotropy, which collectively is in line with previous reports on graphite-based materials.[49,70–73]

The directly-excited ^{15}N MAS NMR spectrum of N-doped C (NH_3) is presented in Fig. 2c. Although this experimental approach is very challenging due to the natural abundance of ^{15}N being only 0.37%, it allows the detection of all types of N sites. We note that the ^{15}N MAS NMR spectrum of Fig. 2c might not be quantitative due to the short relaxation interval employed, however, the choice of such compromise is supported by the relatively fast ^{13}C T_1 relaxation indicating the presence of paramagnetic centers (Fig. S4†). In our previous report on a related N-doped carbon catalyst,[49] we could only detect pyridinic and pyrrolic groups with signal positions in excellent agreement with chemical shifts calculated on the respective models at the reliable DSD-PBEP86/pcS-2 level of theory.[74,75] Serendipitously, the N-doped carbon (NH_3) showed a significantly different ^{15}N MAS NMR spectrum. It contains five distinct ^{15}N resonances as can be observed in Fig. 2c, and the corresponding models with calculated chemical shifts (based on our previous work[49]) are shown above the spectrum. The signals at −74, −275, and −332 ppm could be unambiguously assigned to pyridinic N, pyrrolic N and –NH_2, respectively. The resonance at −21 ppm originates probably from the oxidized nitrogen species, since its chemical shift is close to that of the nitromethane reference at 0 ppm. However, the unexpected broad signal between −160 and −180 ppm was here attributed to graphitic N. As indicated by the structural model, the chemical shifts of such N environments depend on the position of the N atom with respect to the carbon edge.[76] The electronic environments might also be perturbed further by neighbouring structural motifs and result in a broad ^{15}N NMR chemical shift distribution. Irrespectively, to the best of our knowledge, this observation of graphitic N is unprecedented at natural ^{15}N isotope abundance. This shows, in turn, that ^{15}N ssNMR spectroscopy can likely be applied on all types of N-doped carbons with sufficient N-content without expensive and tedious ^{15}N isotope labelling, given that the nitrogen relaxation properties are favorable. Specific to N-doped carbon (NH_3), the combination of ^{15}N ssNMR spectroscopy and quantum chemical shift data showed a structure–property relationship when it came to the graphitic N and the electrocatalytic selectivity in nitrite reduction. The analysis and interpretation of the ^{15}N ssNMR spectrum were fully corroborated by the complementary XPS analysis. However, we cannot exclude a degree of clustering of N atoms in the N-doped carbon (NH_3), as the resonance for graphitic N was broad and a very weak signal at −110 ppm was observed, which could have stemmed from the clustering of pyridinic N with pyrrolic N.[48]

The XPS method gave additional insight into the distribution of N moieties formed on the surface of N-doped C (NH_3). Consistent with the ssNMR results, it showed a comparatively large amount of graphitic N, which accounts for almost 35% of all N atoms. As would be expected, much of the N atoms remained incorporated in the pyridine and pyrrole-type moieties. There are features of four different types of N moieties in the XPS N 1s spectrum in Fig. 3: pyridinic (peak at 398.4 eV), pyrrolic (400.2 eV), graphitic (401.0 eV) and oxidized (403.2 eV).[77] The relative contents of these individual N forms are given in Table 2. The complementary N-doped C (N_2) XPS

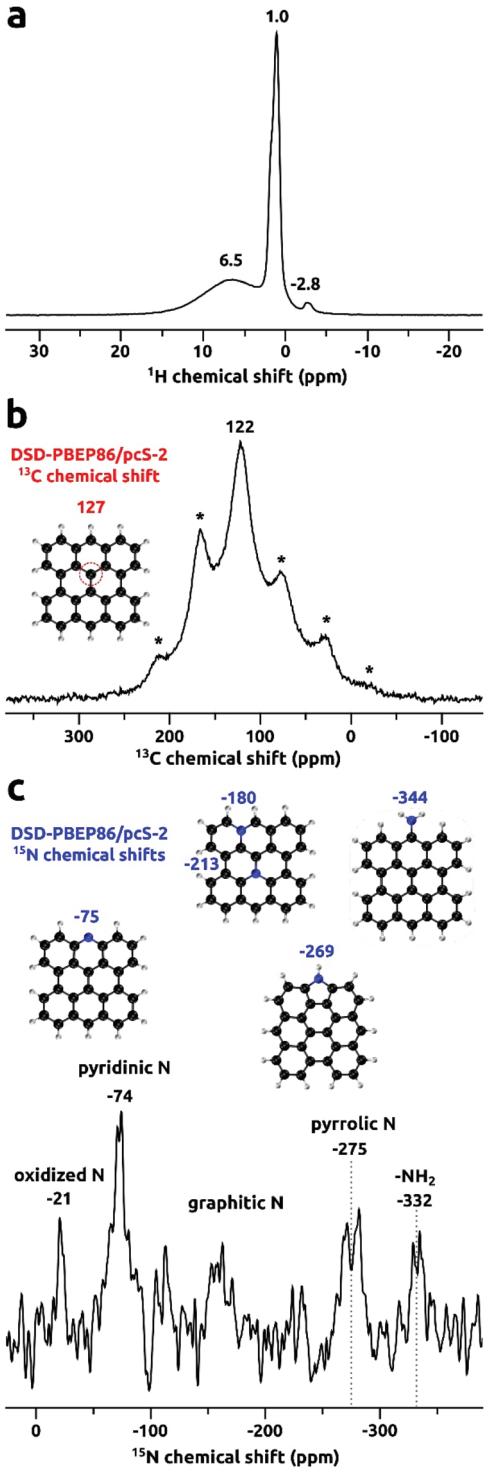

Fig. 2 NMR spectra of N-doped C (NH_3): (a) ^{1}H MAS NMR spectrum at a 60 kHz MAS rate and magnetic field strength of 14.1 T. Directly excited ^{13}C (b) and ^{15}N (c) MAS NMR spectra collected at 7 kHz MAS and 14.1 T, shown together with chemical shifts (in ppm) calculated for hypothetical structural motifs. Experimental chemical shifts are given in black, calculated ^{13}C shifts are in red, and ^{15}N shifts are in blue. The DFT-derived shifts are based on a previous work of the authors.

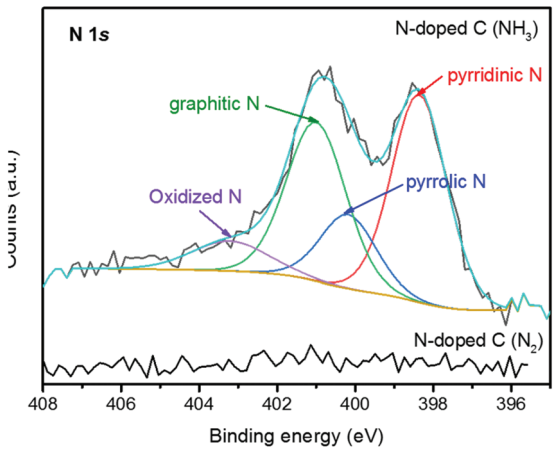

Fig. 3 XPS N 1s spectra of studied N-doped C (NH_3) and N-doped C (N_2).

Table 2 Distribution of different types of N species and their relative contents for N-doped C (NH_3) from XPS

N species (at%)				
Pyridinic	Pyrrolic	Graphitic	Oxidized	Total N
2.82	1.02	2.34	0.56	6.74

N 1s spectrum is characterized by a very low signal-to-noise ratio, and the potential nitrogen signals are lost in the baseline (Fig. 3). This shows that ammonolysis is required to obtain higher nitrogen contents in these materials.

In the Raman spectra (Fig. 4) of both N-doped C (NH_3) and N-doped C (N_2), D and G bands were observed at 1360 cm^{-1} and 1575 cm^{-1}, respectively. The D band is associated with the disordered sp^2 hybridized carbon, while the G band arises from the crystalline graphitic carbon.[78] The intensity ratio of D and G bands (I_D/I_G) is used to assess the degree of graphitization of porous carbon materials.[79] The I_D/I_G ratio of N-doped C (NH_3) (0.948) was higher than that of N-doped C (N_2) (0.740),

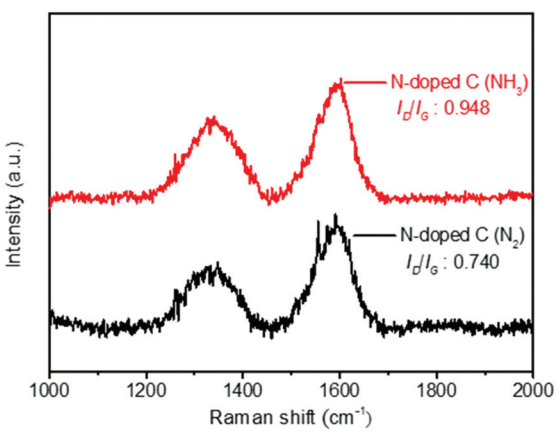

Fig. 4 Raman spectra of N-doped C (N_2) and N-doped C (NH_3).

indicating more defects and disordered structures, which have been suggested to be beneficial for applications in electrocatalysis.[13,63,64] The PXRD patterns for N-doped C (NH_3) and N-doped C (N_2) were similar and showed two broad diffraction peaks at 24° and 44°, which were assigned to the graphite facets (002) and (101) of carbon (Fig. S5†).

Textural data and EM study

The N_2 adsorption/desorption isotherms for N-doped C (N_2) and N-doped C (NH_3) are presented in Fig. 5. Both catalysts showed type I isotherms of microporous materials,[80] and were apparently independent of whether N_2 or NH_3 had been used for the carbonization of cellulose. The specific surface area was slightly higher for N-doped C (NH_3) than for N-doped C (N_2) (S_{BET} = 557 $m^2\ g^{-1}$; $S_{Langmuir}$ = 669 $m^2\ g^{-1}$). It is most likely that the treatment of cellulose with HNO_3 followed by carbonization in flowing NH_3/H_2 led to the formation of wide pores (mesopores) and, as a result, an increase in the total pore volume. A similar effect has been observed previously for sucrose-derived carbon replicas.[49] The textural data derived *via* N_2 adsorption/desorption experiments under cryogenic conditions are displayed in Table 3.

The features observed in the SEM micrographs (Fig. 6a and b) confirm the irregularity in the shape of the particles of N-doped C (NH_3) and N-doped C (N_2). However, the size of the particles was smaller for N-doped C (NH_3) as is visible from the SEM micrographs at lower magnification (Fig. S6†). The complementary morphological analysis of N-doped C (NH_3) by means of TEM provides evidence of a high degree of porosity with pore sizes of app. 1–2 nm (Fig. 6c and d), which was consistent with the analysis of N_2 adsorption/desorption data. Moreover, structural analysis by TEM and XPS indicates that the textural characteristics of the N-doped C (NH_3) catalyst remain unchanged and its structural stability is maintained after the electrocatalytic tests (Fig. S7†). It should be noted that the XPS spectrum in Fig. S7† was collected on the complete composite electrode instead of the N-doped carbon powder. As such, the signal-to-noise ratio is smaller and only the graphitic and pyridinic nitrogen signals could be detected.

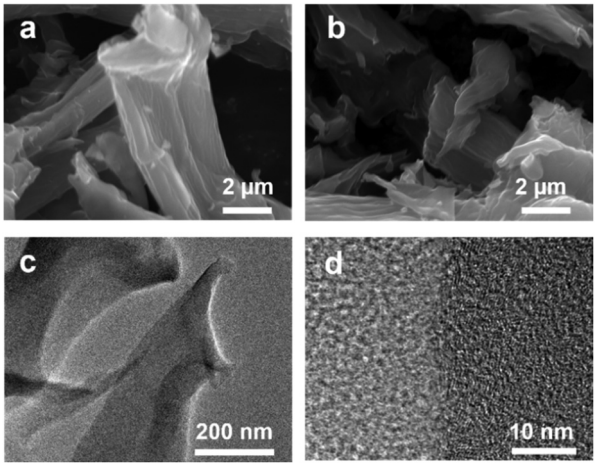

Fig. 6 SEM micrographs of N-doped C (NH_3) (a) and N-doped C (N_2) (b); (c, d) TEM images of N-doped C (NH_3).

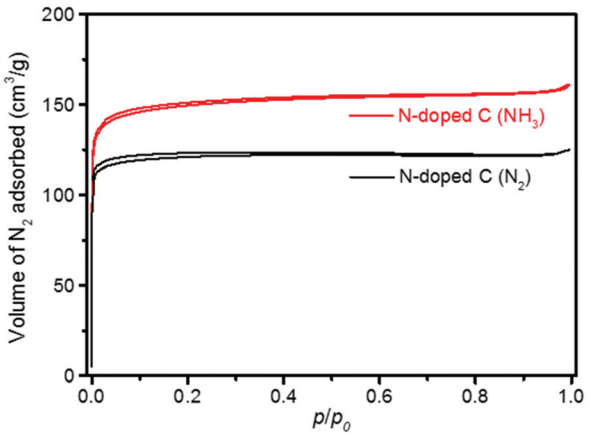

Fig. 5 N_2 adsorption–desorption isotherms of N-doped C (N_2) and N-doped C (NH_3).

Table 3 Textural parameters and N content from the elemental analysis of N-doped C (N_2) and N-doped C (NH_3)

Sample	S_{BET} ($m^2\ g^{-1}$)	$S_{Langmuir}$ ($m^2\ g^{-1}$)	V_{total} ($cm^3\ g^{-1}$)	V_{meso} ($cm^3\ g^{-1}$)	V_{micro} ($cm^3\ g^{-1}$)	N content (wt%)
N-Doped C (N_2)	452	534	0.19	0.006	0.17	0.6
N-Doped C (NH_3)	557	669	0.25	0.022	0.20	6.5

Elemental analysis

The developed procedure of cellulose carbonization, including initial oxidation with nitric acid and then ammonolysis at 800 °C, allowed the incorporation of 6.5 wt% of N into N-doped C (NH_3), while N-doped C (N_2) had only 0.6 wt% of

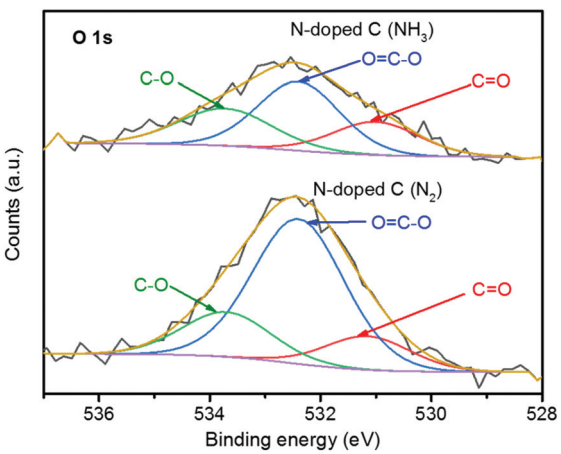

Fig. 7 XPS O 1s spectra of both studied N-doped C samples.

Table 4 Distribution of different types of O species on N-doped C (N_2) and N-doped C (NH_3)

	O species (at%)			
Sample	C═O	O═C–O	C–O	Total O
N-Doped C (N_2)	0.49	2.26	0.68	3.43
N-Doped C (NH_3)	0.50	0.98	0.61	2.09

N. N-doped C had the metal content of Cu, Co, Cr, Mn, Mo, Ni, V, W, Pt and Pd of < 10 ppm.

The surfaces of the N-doped C (NH_3) and N-doped C (N_2) catalysts contained a significant amount of O atoms, and XPS allowed three different forms of such O atoms to be recognized. The photoemissions at 531.1, 532.4 and 533.7 eV in the O 1s spectra (Fig. 7) were assigned to O in C═O (carbonyls), O═C–O (esters, anhydrides and carboxylic acids) and C–O (phenols and ethers), respectively.[81] N-doped C (N_2) had more O atoms than N-doped C (NH_3) (Table 4), with a total amount of 3.43 at% of surface O atoms, with predominantly carboxyl groups (66% of all O atoms). The reducing atmosphere (NH_3/H_2) during the preparation of N-doped C (NH_3) seems to have suppressed the oxygenation of the surface.

Conclusions

The N-doped carbon catalyst prepared from cellulose with a combination of HNO_3 treatment and ammonolysis had a high N content. It showed a higher electrocatalytic activity for the OER, HER, and nitrate reduction as compared with the reference material prepared by the carbonization of HNO_3 treated cellulose in N_2. The enhanced activity of N-doped C (NH_3) was related to the high content of 6.5 wt% N, and the improved catalytic activity under alkaline conditions was tentatively related to the type of nitrogen function. Its high selectivity in the electrochemical reduction of nitrite was related to graphitic N, since pyridinic N and pyrrolic N had earlier been shown to not affect the electrochemical reduction of nitrite. The inclusion of graphitic N was ascribed to the comparably high temperature of ammonolysis and/or the use of cellulose as a carbon source. The presence of graphitic N in N-doped C (NH_3) was determined by means of directly-excited ^{15}N ssNMR spectroscopy.

Our study highlights the potential of using ^{15}N ssNMR spectroscopy at natural ^{15}N isotope abundance for a wide range of materials. Specifically, we identify the structure–property relationship for graphitic N and the enhanced selectivity in the electrochemical reduction of nitrite without costly and often tedious ^{15}N labelling. The methodology provides such an opportunity to determine the local chemistry around N at the atomic level and to establish a structure–property relationship with respect to its catalytic activity in general. The serendipitous discovery of graphitic N in N-doped catalysts derived from cellulose has further potential for the synthesis of metal-free catalysts using renewable substrates. Further studies on the synthesis of carbon materials with solely graphitic N are currently being carried out in our laboratories.

Conflicts of interest

There are no conflicts to declare.

Acknowledgements

Z. C. thanks the China Scholarship Council for a PhD scholarship. P. K. acknowledges the European Regional Development Fund in the framework of the Polish Innovation Operational Program (contract no. POIG.02.01.00-12-023/08) for financial support. We are indebted to Serhiy Budnyk for ICP analyses and Jedrzej Piatek for fruitful discussions. We thank the Swedish Foundation for Strategic Environmental Research (project: Mistra SafeChem, project number 2018/11) for financial support.

References

1 H. Tan, Y. Zhao, W. Xia, J. Zhao, X. Xu, K. Wood, Y. Sugahara, Y. Yamauchi and J. Tang, *Chem. Mater.*, 2020, **32**, 4248–4256.
2 G. H. Wang, Z. Cao, D. Gu, N. Pfänder, A. C. Swertz, B. Spliethoff, H. J. Bongard, C. Weidenthaler, W. Schmidt, R. Rinaldi and F. Schüth, *Angew. Chem., Int. Ed.*, 2016, **55**, 8850–8855.
3 C. Lu, P. R. Jothi, T. Thersleff, T. M. Budnyak, A. Rokicinska, K. Yubuta, R. Dronskowski, P. Kuśtrowski, B. P. T. Fokwa and A. Slabon, *Nanoscale*, 2020, **12**, 3121–3128.
4 G. J. F. Cruz, L. Kuboňová, D. Y. Aguirre, L. Matějová, P. Peikertová, I. Troppová, E. Cegmed, A. Wach, P. Kustrowski, M. M. Gomez and L. Obalová, *ACS Sustainable Chem. Eng.*, 2017, **5**, 2368–2374.
5 G. Mestl, N. I. Maksimova, N. Keller, V. V. Roddatis and R. Schlögl, *Angew. Chem., Int. Ed.*, 2001, **40**, 2066–2068.
6 R. Pawlak, X. Liu, S. Ninova, P. D'Astolfo, C. Drechsel, S. Sangtarash, R. Haner, S. Decurtins, H. Sadeghi, C. J. Lambert, U. Aschauer, S.-X. Liu and E. Meyer, *J. Am. Chem. Soc.*, 2020, **142**, 12568–12573.
7 J. Zhang, Y. Zhao, C. Chen, Y.-C. Huang, C.-L. Dong, C.-J. Chen, R.-S. Liu, C. Wang, K. Yan, Y. Li and G. Wang, *J. Am. Chem. Soc.*, 2019, **141**, 20118–20126.
8 K. Yuan, D. Lutzenkirchen-Hecht, L. Li, L. Shuai, Y. Li, R. Cao, M. Qiu, X. Zhuang, M. K. H. Leung, Y. Chen and U. Scherf, *J. Am. Chem. Soc.*, 2020, **142**, 2404–2412.
9 H. W. Kim, H. Park, J. S. Roh, J. E. Shin, T. H. Lee, L. Zhang, Y. H. Cho, H. W. Yoon, V. J. Bukas, J. Guo, H. B. Park, T. H. Han and B. D. McCloskey, *Chem. Mater.*, 2019, **31**, 3967–3973.

10 H. Wang, Y. Shao, S. Mei, Y. Lu, M. Zhang, J.-K. Sun, K. Matyjaszewski, M. Antonietti and J. Yuan, *Chem. Rev.*, 2020, **120**, 9363–9419.
11 H. Wang, J. Jia, P. Song, Q. Wang, D. Li, S. Min, C. Qian, L. Wang, Y. F. Li, C. Ma, T. Wu, J. Yuan, M. Antonietti and G. A. Ozin, *Angew. Chem., Int. Ed.*, 2017, **56**, 7847–7852.
12 X. Hu, L. Zhong, C. Shu, Z. Fang, M. Yang, J. Li and D. Yu, *J. Am. Chem. Soc.*, 2020, **142**, 4621–4630.
13 K. Tian, J. Wang, L. Cao, W. Yang, W. Guo, S. Liu, W. Li, F. Wang, X. Li, Z. Xu, Z. Wang, H. Wang and Y. Hou, *Nat. Commun.*, 2020, **11**, 3884.
14 J. Zhang, Z. Zhao, Z. Xia and L. Dai, *Nat. Nanotechnol.*, 2015, **10**, 444–452.
15 X. Wang, A. Vasileff, Y. Jiao, Y. Zheng and S.-Z. Qiao, *Adv. Mater.*, 2019, **31**, 1803625.
16 X.-Y. Wang, X. Yao, A. Narita and K. Müllen, *Acc. Chem. Res.*, 2019, **52**, 2491–2505.
17 D. Liu, L. Dai, X. Lin, J.-F. Chen, J. Zhang, X. Feng, K. Müllen, X. Zhu and S. Dai, *Adv. Mater.*, 2019, **31**, 1804863.
18 J. B. Zimmerman, P. T. Anastas, H. C. Erythropel and W. Leitner, *Science*, 2020, **367**, 397–400.
19 J. T. Grant, C. A. Goeltl, F. Goeltl, J. Venegas, P. Mueller, S. P. Burt, S. E. Specht, W. P. McDermott, A. Chieregato and I. Hermans, *Science*, 2016, **354**, 1570–1573.
20 Y. Subaşı, M. Somer, M. B. Yağcı, A. Slabon and S. Afyon, *J. Solid State Electrochem.*, 2020, **24**, 1085–1093.
21 W. Hao, N. Keshavarzi, A. Branger, L. Bergström and N. Hedin, *Carbon*, 2014, **78**, 521–531.
22 X. Zhao, P. Pachfule, S. Li, T. Langenhahn, M. Ye, G. Tian, J. Schmidt and A. Thomas, *Chem. Mater.*, 2019, **31**, 3274–3280.
23 C. Galeano, J. C. Meier, M. Soorholtz, H. Bongard, C. Baldizzone, K. J. J. Mayrhofer and F. Schüth, *ACS Catal.*, 2014, **4**, 3856–3868.
24 D. Deng, X. Pan, L. Yu, Y. Cui, Y. Jiang, J. Qi, W.-X. Li, Q. Fu, X. Ma, Q. Xue, G. Sun and X. Bao, *Chem. Mater.*, 2011, **23**, 1188–1193.
25 C. Maddi, F. Bourquard, V. Barnier, J. Avila, M.-C. Asensio, T. Tite, C. Donnet and F. Garrelie, *Sci. Rep.*, 2018, **8**, 3247.
26 T. Schiros, D. Nordlund, L. Pálová, D. Prezzi, L. Zhao, K. S. Kim, U. Wurstbauer, C. Gutiérrez, D. Delongchamp, C. Jaye, D. Fischer, H. Ogasawara, L. G. M. Pettersson, D. R. Reichman, P. Kim, M. S. Hybertsen and A. N. Pasupathy, *Nano Lett.*, 2012, **12**, 4025–4031.
27 H. Luo, S. Dimitrov, M. Daboczi, J.-S. Kim, Q. Guo, Y. Fang, M.-A. Stoeckel, P. Samorì, O. Fenwick, A. B. J. Sobrido, X. Wang and M.-M. Titirici, *ACS Appl. Nano Mater.*, 2020, **3**, 3371–3381.
28 J. Li, L. Jiao, E. Wegener, L. L. Richard, E. Liu, A. Zitolo, M. T. Sougrati, S. Mukerjee, Z. Zhao, Y. Huang, F. Yang, S. Zhong, H. Xu, A. J. Kropf, F. Jaouen, D. J. Myers and Q. Jia, *J. Am. Chem. Soc.*, 2020, **142**, 1417–1423.
29 L. Wang, Z. Sofer and M. Pumera, *ACS Nano*, 2020, **14**, 21–25.
30 M. Borghei, J. Lehtonen, L. Liu and O. J. Rojas, *Adv. Mater.*, 2018, **30**, 1703691.
31 H. Begum, M. S. Ahmed and Y.-B. Kim, *Sci. Rep.*, 2020, **10**, 12431.
32 L. Xu, Q. Yao, Y. Zhang and Y. Fu, *ACS Sustainable Chem. Eng.*, 2017, **5**, 2960–2969.
33 B. You, F. Kang, P. Yin and Q. Zhang, *Carbon*, 2016, **103**, 9–15.
34 B. You, P. Yin, J. Zhang, D. He, G. Chen, F. Kang, H. Wang, Z. Deng and Y. Li, *Sci. Rep.*, 2015, **5**, 1–9.
35 B. You, P. Yin and L. An, *Small*, 2014, **10**, 4352–4361.
36 J. Zhang, G. Chen, Q. Zhang, F. Kang and B. You, *ACS Appl. Mater. Interfaces*, 2015, **7**, 12760–12766.
37 B. You, X. Liu, G. Hu, S. Gul, J. Yano, D. E. Jiang and Y. Sun, *J. Am. Chem. Soc.*, 2017, **139**, 12283–12290.
38 M. Soorholtz, R. J. White, T. Zimmermann, M.-M. Titirici, M. Antonietti, R. Palkovits and F. Schüth, *Chem. Commun.*, 2013, **49**, 240–242.
39 K. Qu, Y. Zheng, X. Zhang, K. Davey, S. Dai and S. Z. Qiao, *ACS Nano*, 2017, **11**, 7293–7300.
40 L. Zhao, N. Baccile, S. Gross, Y. Zhang, W. Wei, Y. Sun, M. Antonietti and M.-M. Titirici, *Carbon*, 2010, **48**, 3778–3787.
41 H. Jiang, J. Gu, X. Zheng, M. Liu, X. Qiu, L. Wang, W. Li, Z. Chen, X. Ji and J. Li, *Energy Environ. Sci.*, 2019, **12**, 322–333.
42 Y. Zhao, R. Nakamura, K. Kamiya, S. Nakanishi and K. Hashimoto, *Nat. Commun.*, 2013, **4**, 2390.
43 J. H. Warner, Y.-C. Lin, K. He, M. Koshino and K. Suenaga, *ACS Nano*, 2014, **8**, 11806–11815.
44 C. Hofer, V. Skákalová, T. Görlich, M. Tripathi, A. Mittelberger, C. Mangler, M. R. A. Monazam, T. Susi, J. Kotakoski and J. C. Meyer, *Nat. Commun.*, 2019, **10**, 4570.
45 X. Li, I. V. Sergeyev, F. Aussenac, A. F. Masters, T. Maschmeyer and J. M. Hook, *Angew. Chem., Int. Ed.*, 2018, **57**, 6848–6852.
46 Y. Hu, Y. Shim, J. Oh, S. Park, S. Park and Y. Ishii, *Chem. Mater.*, 2017, **29**, 5080–5089.
47 S. Kuroki, Y. Hosaka and C. Yamauchi, *Carbon*, 2013, **55**, 160–167.
48 X. Fang, J. Mao, E. M. Levin and K. Schmidt-Rohr, *J. Am. Chem. Soc.*, 2009, **131**, 1426–1435.
49 I. Szewczyk, A. Rokicińska, M. Michalik, J. Chen, A. Jaworski, R. Aleksis, A. J. Pell, N. Hedin, A. Slabon and P. Kuśtrowski, *Chem. Mater.*, 2020, **32**, 7263–7273.
50 W. Luo, B. Wang, C. G. Heron, M. J. Allen, J. Morre, C. S. Maier, W. F. Stickle and X. Ji, *Nano Lett.*, 2014, **14**, 2225–2229.
51 X. Wu, Z. Shi, R. Tjandra, A. J. Cousins, S. Sy, A. Yu, R. M. Berry and K. C. Tam, *J. Mater. Chem. A*, 2015, **3**, 23768–23777.
52 X. Du, Z. Zhang, W. Liu and Y. Deng, *Nano Energy*, 2017, **35**, 299–320.
53 A. Wütscher, T. Eckhard, D. Hiltrop, K. Lotz, W. Schuhmann, C. Andronescu and M. Muhler, *ChemElectroChem*, 2019, **6**, 514–521.
54 B. P. Chhetri, D. Soni, A. B. RanguMagar, C. M. Parnell, H. Wayland, F. Watanabe, G. Kannarpady, A. S. Biris and A. Ghosh, *J. Environ. Chem. Eng.*, 2017, **5**, 2586–2596.
55 S. Zuo, W. Zhang, Y. Wang and H. Xia, *Ind. Eng. Chem. Res.*, 2020, **59**, 7527–7537.

56 R. Huang, C. Cao, J. Liu, D. Sun and W. Song, *Chem. Commun.*, 2019, **55**, 1935–1938.
57 N. N. Sauer, *J. Am. Chem. Soc.*, 2000, **122**, 5419–5420.
58 Z. Ma, A. Jaworski, J. George, A. Rokicinska, T. Thersleff, T. M. Budnyak, G. Hautier, A. J. Pell, R. Dronskowski, P. Kuśtrowski and A. Slabon, *J. Phys. Chem. C*, 2020, **124**, 152–160.
59 Z. Ma, T. Thersleff, A. L. Görne, N. Cordes, Y. Liu, S. Jakobi, A. Rokicinska, Z. G. Schichtl, R. H. Coridan, P. Kustrowski, W. Schnick, R. Dronskowski and A. Slabon, *ACS Appl. Mater. Interfaces*, 2019, **11**, 19077–19086.
60 T.-L. Hwang, P. C. M. van Zijl and M. Garwood, *J. Magn. Reson.*, 1998, **133**, 200–203.
61 G. Kervern, G. Pintacuda and L. Emsley, *Chem. Phys. Lett.*, 2007, **435**, 157–162.
62 Y. Zhao, R. Shi, X. Bian, C. Zhou, Y. Zhao, S. Zhang, F. Wu, G. I. N. Waterhouse, L.-Z. Wu, C.-H. Tung and T. Zhang, *Adv. Sci.*, 2019, **6**, 1802109.
63 Z. Luo, S. Lim, Z. Tian, J. Shang, L. Lai, B. MacDonald, C. Fu, Z. Shen, T. Yu and J. Lin, *J. Mater. Chem.*, 2011, **21**, 8038–8044.
64 Q. Lv, W. Si, J. He, L. Sun, C. Zhang, N. Wang, Z. Yang, X. Li, X. Wang, W. Deng, Y. Long, C. Huang and Y. Li, *Nat. Commun.*, 2018, **9**, 3376.
65 J. J. Ternero-Hidalgo, J. M. Rosas, J. Palomo, M. J. Valero-Romero, J. Rodríguez-Mirasol and T. Cordero, *Carbon*, 2016, **101**, 409–419.
66 A. R. MacIntosh, G. Jiang, P. Zamani, Z. Song, A. Riese, K. J. Harris, X. Fu, Z. Chen, X. Sun and G. R. Goward, *J. Phys. Chem. C*, 2018, **122**, 6593–6601.
67 A. C. Forse, J. M. Griffin, V. Presser, Y. Gogotsi and C. P. Grey, *J. Phys. Chem. C*, 2014, **118**, 7508–7514.
68 L. Cervini, O. D. Lynes, G. R. Akien, A. Kerridge, N. S. Barrow and J. M. Griffin, *Energy Storage Mater.*, 2019, **21**, 335–346.
69 P. v. R. Schleyer, C. Maerker, A. Dransfeld, H. Jiao and N. J. R. van Eikema Hommes, *J. Am. Chem. Soc.*, 1996, **118**, 6317–6318.
70 A. Lerf, H. He, T. Riedl, M. Forster and J. Klinowski, *Solid State Ionics*, 1997, **101**, 857–862.
71 A. Lerf, H. He, M. Forster and J. Klinowski, *J. Phys. Chem. B*, 1998, **102**, 4477–4482.
72 Y. Li, H. Chen, L. Y. Voo, J. Ji, G. Zhang, G. Zhang, F. Zhang and X. Fan, *J. Mater. Chem.*, 2012, **22**, 15021–15024.
73 Q. Zhang, K. Scrafford, M. Li, Z. Cao, Z. Xia, P. M. Ajayan and B. Wei, *Nano Lett.*, 2014, **14**, 1938–1943.
74 G. L. Stoychev, A. A. Auer and F. Neese, *J. Chem. Theory Comput.*, 2018, **14**(9), 4756–4771.
75 P. Rzepka, Z. Bacsik, A. J. Pell, N. Hedin and A. Jaworski, *J. Phys. Chem. C*, 2019, **123**, 21497–21503.
76 S. R. Kelemen, M. Afeworki, M. L. Gorbaty, P. J. Kwiatek, M. S. Solum, J. Z. Hu and R. J. Pugmire, *Energy Fuels*, 2002, **16**, 1507–1515.
77 Y. Cao, S. Mao, M. Li, Y. Chen and Y. Wang, *ACS Catal.*, 2017, **7**, 8090–8112.
78 P. P. Sharma, J. Wu, R. M. Yadav, M. Liu, C. J. Wright, C. S. Tiwary, B. I. Yakobson, J. Lou, P. M. Ajayan and X.-D. Zhou, *Angew. Chem., Int. Ed.*, 2015, **127**, 13905–13909.
79 A. C. Ferrari, *Solid State Commun.*, 2007, **143**, 45–47.
80 K. S. W. Sing, D. H. Everett, R. A. W. Haul, L. Moscou, R. A. Pierotti, J. Rouquerol and T. Siemieniewska, *Pure Appl. Chem.*, 1985, **57**, 603–619.
81 S. Tian, P. Yan, F. Li, X. Zhang, D. Su and W. Qi, *ChemCatChem*, 2019, **11**, 2073–2078.

